3
Development of Cutting Force Model

3.1 INTRODUCTION

Cutting force is the primary source of multiple faults that deteriorates the quality of machined component during the end milling operation. The estimation, monitoring, and control of cutting force are imperative to avoid or minimize faults such as tool breakage, tool wear, selection of inappropriate cutting parameters, fixture errors, etc. The reliable estimation of cutting forces is substantially important in this thesis work while developing a computational framework for modeling and control of geometric tolerances in the subsequent chapters. The cutting force in flat end milling operation is contributed by the involvement of flank and bottom cutting edges as depicted in Figure 3.1.

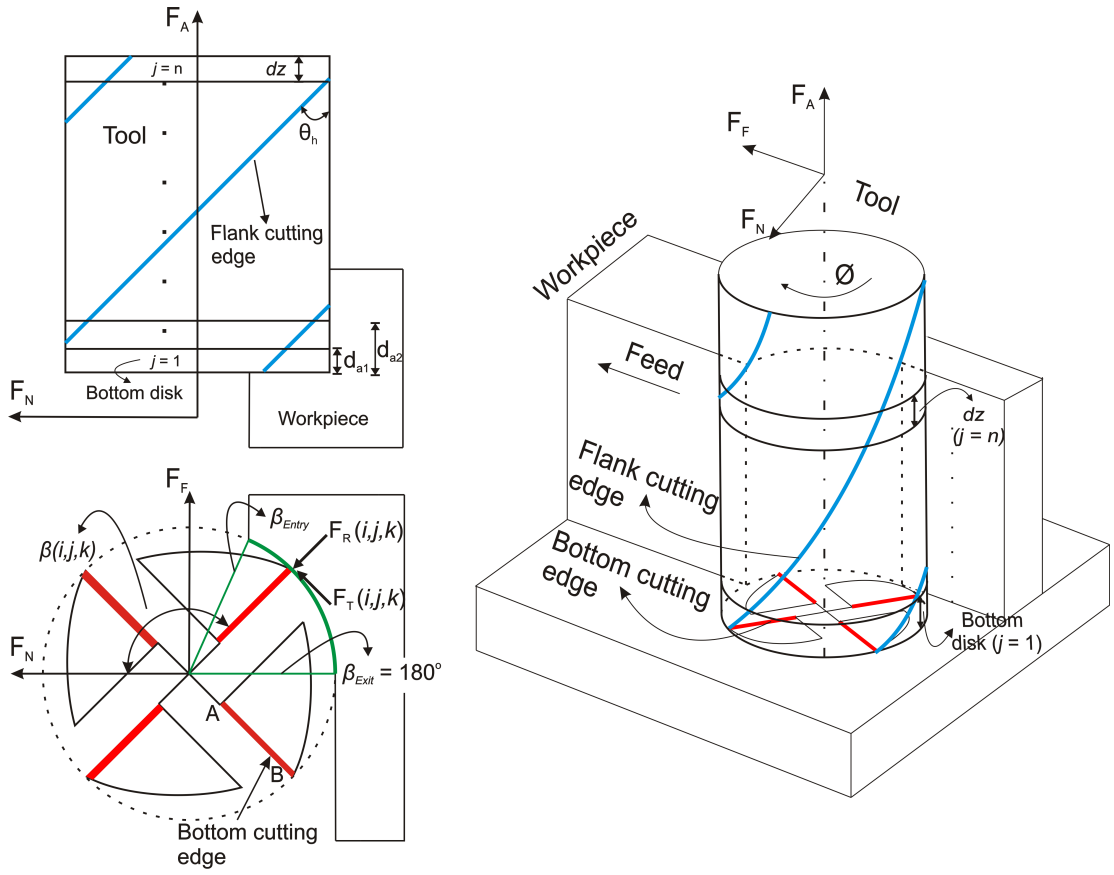

Figure 3.1 : Schematic Illustration of Cutting Edges and Process Geometry Parameters in End Milling

It was realized that the relative contribution of flank and bottom edges towards total cutting force in the flat end milling has not been studied in the literature over a range of cutting widths i.e. *ADOC* and *RDOC*. It is necessary to examine the applicability of predictive force models over a wide range of cutting widths, which would assist while developing effective models for estimating and controlling geometric tolerances. It was highlighted in Chapter 2 that the mechanistic

force model is popular among the researchers and can predict cutting forces with reasonable accuracy in comparison to other methodologies with the requirement of fewer experiments for the conditioning. The mechanistic model determines the uncut chip area geometrically and correlates it with the cutting force components using a set of cutting constants. Also, the determination of cutting constants is quite complex as the process is solely dependent on experimentally measured force data and the relationship comprehends the effect of various process attributes.

In this context, a comparative assessment of three different analytical approaches highlighting the importance of incorporating bottom and flank cutting edges in cutting force model for flat-end milling operation is presented in this chapter. The study focuses on identifying the most appropriate method that includes the effect of cutting edges and predicts accurately over a wide range of cutting widths, i.e., *ADOC* and *RDOC*. The first approach uses the average cutting constants directly estimated from the experimental force data [Wan et al., 2008a]. The second approach pre-processes the experimental data to exclude the contribution of bottom edges and determine constants associated with the flank for estimation of cutting forces [Ko et al., 2002]. The third approach considers the systematic derivation of independent constants for the flank and bottom cutting edges followed by summation of individual contributions to determine the total cutting force [Dang et al., 2010]. The present work implements these approaches in the form of computational models, and machining experiments are conducted subsequently to examine the efficacy of proposed methods in estimating cutting force for flat-end milling operation. The primary objective of this analysis is to examine the importance of the flank and bottom cutting edges over a wide range of cutting widths and select an appropriate variant subsequently.

The application of data-driven or machine learning models is becoming popular in recent times for analyzing various manufacturing process attributes. The data-driven models use input and output datasets to evolve relationships similar to human perceptions. The development of a reliable data-driven model is challenging due to the necessity of conducting numerous experiments for the generation of datasets, the presence of outliers and noise in the datasets, process disturbances, etc., but it can be scaled easily by accommodating new variables and attributes to evolve progressively. Alternatively, physics-based models establish an explicit relationship of process variables with the desired attributes based on scientific knowledge and assumptions, but the scalability is difficult. The present work also explores the development of a hybrid cutting force model that amalgamates a physics-based approach to evaluate chip geometry and a machine learning-based approach to determine cutting constants. The cutting forces obtained using the proposed hybrid approach are compared with an ideal analytical approach selected previously by performing a set of computational studies and milling experiments.

3.2 MECHANISTIC FORCE MODEL

The mechanistic force model discretizes flat-end mill into a finite number of disk elements having an equal thickness (dz) and evaluates the engagement state of each cutting tooth at a given cutter rotation angle. Subsequently, the model correlates the uncut chip area with elemental cutting force components using mechanistic cutting constants (K_T, K_R and K_A). The tangential (F_T), radial (F_R) and axial (F_A) cutting force components corresponding to k^{th} engaged flute on j^{th} axial disk element at cutter rotation angle (ϕ_i) can be expressed using Eq. 3.1 and as depicted in Figure 3.1. The instantaneous uncut chip thickness $t_c(i,j,k)$ is the shortest distance between two consecutive tooth passes at a given angular position of the disk element and it can be expressed geometrically using Eq. 3.2 as a function of feed per tooth (f_{pt}). The angular position $\beta(i,j,k)$ of each axial disk element and cutting teeth is dependent on the tooth spacing angle (θ_c) and helix angle (θ_h) of end mill and it can be determined using Eq. 3.3.

$$\begin{bmatrix} F_T(i,j,k) \\ F_R(i,j,k) \\ F_A(i,j,k) \end{bmatrix} = dz\, t_c(i,j,k) \begin{bmatrix} K_T(i,j,k) \\ K_R(i,j,k) \\ K_A(i,j,k) \end{bmatrix} \tag{3.1}$$

$$t_c(i,j,k) = f_{pt}\, sin\, \beta(i,j,k) \tag{3.2}$$

$$\beta(i,j,k) = \phi_i + (k-1)\,\theta_c + \left((j-1)\,dz + \frac{dz}{2}\right) \frac{tan\,(\theta_h)}{R_c} \tag{3.3}$$

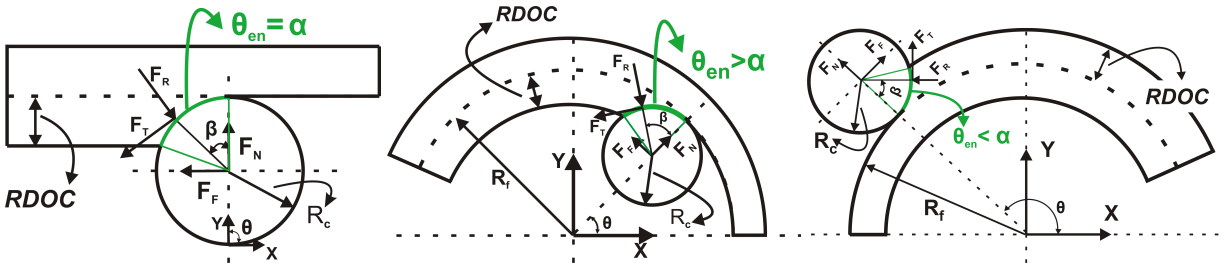

Figure 3.2 : Illustration for End Milling of Different Geometries

The present thesis work considers the machining of straight, concave and convex thin-walled components, which differs in cutting configurations as depicted in Figure 3.2. The circular geometry has a constant radius of curvature in comparison to straight geometries having no curvature. Therefore, a generic cutting force model incorporating the effect of variation in workpiece geometry is used in the present study. The f_{pt} in the case of circular component is not the identical to the actual or programmed feed per tooth (f_a) and depends upon the nature of workpiece curvature (concave or convex) and magnitude of the radius of curvature. Similarly, the engagement angle (θ_{en}) also changes with the geometry of the workpiece due to change in the dimensions of the transition area as depicted in Figure 3.2. The mathematical formulation for f_{pt} and θ_{en} during machining of straight, concave and convex geometry are given in Table 3.1 Here, R_f and R_c represents the final radius of the curvature of the workpiece and radius of the cutter respectively.

Table 3.1 : Process Geometry Parameters for Straight and Circular Components

Geometry	Feed per tooth (f_{pt})	Engagement Angle (θ_{en})
Straight	f_a	$cos^{-1}\left(1 - \frac{RDOC}{R_c}\right)$
Concave	$f_a\left(\frac{R_f - RDOC}{R_f - R_c}\right)$	$cos^{-1}\left(\frac{R_c^2 + (R_f - R_c)^2 - (R_f - RDOC)^2}{2R_c(R_f - R_c)}\right)$
Convex	$f_a\left(\frac{R_f + RDOC}{R_f + R_c}\right)$	$cos^{-1}\left(\frac{R_c^2 + (R_f + R_c)^2 - (R_f + RDOC)^2}{2R_c(R_f + R_c)}\right)$

The total cutting force acting in the Feed (F_F), Normal (F_N) and Axial (F_A) directions at a cutter rotation angle (ϕ_i) can be obtained by resolving the elemental components into feed, normal, and axial directions using 3-D transformations. Equation 3.4 represents mathematical formulation to transform the forces into the feed and normal directions at an element level. Equation 3.5

represent mathematical formulation to determine the total cutting force at the cutter rotation angle (ϕ_i) by summation of forces acting on each engaged disk element and cutting teeth. The magnitude of cutting force in the axial direction (F_A) is negligible in comparison to the feed (F_F) and normal (F_N) components for flat-end milling operation. Therefore it is not considered in the present work. Equation 3.6 presents the cutting force system reduced to two components. The cutting force obtained in the normal (F_N) direction subtends an angle θ with the X- axis as shown in Figure 3.2 for all three geometries. The angle facilitates the transformation of feed (F_F) and normal (F_N) component of the forces into the global coordinate system (X- and Y- forces) using Eq. 3.7. The cutting force components in the global coordinate system are used subsequently while developing an overall framework.

$$\begin{bmatrix} F_F(i,j,k) \\ F_N(i,j,k) \\ F_A(i,j,k) \end{bmatrix} = dz\, t_c(i,j,k) \begin{bmatrix} cos\,\beta(i,j,k) & -sin\,\beta(i,j,k) & 0 \\ sin\,\beta(i,j,k) & cos\,\beta(i,j,k) & 0 \\ 0 & 0 & 1 \end{bmatrix} \begin{bmatrix} F_T(i,j,k) \\ F_R(i,j,k) \\ F_A(i,j,k) \end{bmatrix} \tag{3.4}$$

$$\begin{bmatrix} F_F(\phi_i) \\ F_N(\phi_i) \\ F_A(\phi_i) \end{bmatrix} = \sum_{j,k} dz \begin{bmatrix} cos\,\beta(i,j,k)\, t_c(i,j,k) & -sin\,\beta(i,j,k)\, t_c(i,j,k) & 0 \\ sin\,\beta(i,j,k)\, t_c(i,j,k) & cos\,\beta(i,j,k)\, t_c(i,j,k) & 0 \\ 0 & 0 & 1 \end{bmatrix} \begin{bmatrix} K_T(i,j,k) \\ K_R(i,j,k) \\ K_A(i,j,k) \end{bmatrix} \tag{3.5}$$

$$\begin{bmatrix} F_F(\phi_i) \\ F_N(\phi_i) \end{bmatrix} = \sum_{j,k} dz \begin{bmatrix} cos\,\beta(i,j,k)\, t_c(i,j,k) & -sin\,\beta(i,j,k)\, t_c(i,j,k) \\ sin\,\beta(i,j,k)\, t_c(i,j,k) & cos\,\beta(i,j,k)\, t_c(i,j,k) \end{bmatrix} \begin{bmatrix} K_T(i,j,k) \\ K_R(i,j,k) \end{bmatrix} \tag{3.6}$$

$$\begin{bmatrix} F_X(\phi_i) \\ F_Y(\phi_i) \end{bmatrix} = \begin{bmatrix} -sin\,\theta & cos\,\theta \\ cos\,\theta & sin\,\theta \end{bmatrix} \begin{bmatrix} F_F(\phi_i) \\ F_N(\phi_i) \end{bmatrix} \tag{3.7}$$

The cutting constants $K_q(i,j,k)$ $(q = T,R)$ correlate instantaneous uncut chip thickness with cutting forces that are determined by conducting experiments at various cutting conditions for a given tool-workpiece pair. It has been reported in the literature that the prediction accuracy of the mechanistic force model greatly depends on the correctness of cutting constant. The cutting constants capture the effect of various process attributes such as shearing and ploughing phenomenon, tool-workpiece material properties, cut geometry parameters (radial and axial immersions), etc. Therefore, the determination of cutting constants is considered as a critical step in the development of the cutting force model. This thesis work employs analytical and machine learning methods to correlate cutting constants as a function of uncut chip thickness for establishing a non-linear relationship. The uncut chip thickness is a function of cutting parameters such as feed rate, spindle speed, axial and radial immersions, number of flutes, helix angle and diameter of the cutter. Therefore, cutting constants predicted in this study can accommodate variation of these parameters while predicting forces. The subsequent subsections discusses various approaches employed in the thesis work to establish the relationship between cutting constants and instantaneous uncut chip thickness.

3.3 ANALYTICAL APPROACHES FOR ESTIMATION OF CUTTING CONSTANTS

The primary objective of the present thesis work is to predict cutting forces over a wide range of cutting widths, i.e. *ADOC* and *RDOC* therefore, the precise calibration of cutting constants

relationship is of utmost importance. This section presents the procedure for establishing the relationship between cutting constants and instantaneous uncut chip thickness through three different analytical approaches adapted from the literature. The first approach establishes the relationship between average chip thickness and cutting constants derived from measured cutting forces [Wan et al., 2008a]. The second approach considers preprocessing of measured cutting force signal to extract the component contributed by the flank while obtaining cutting constant relationship [Ko et al., 2002]. The third approach considers the determination of flank constants and associated cutting forces similar to the second approach but it considers an additional contribution from the bottom edge while determining total cutting forces [Dang et al., 2010]. These three analytical approaches aim to correlate cutting constants with uncut chip thickness using a curve fitting technique. The fundamental difference among these analytical approaches lies in the process of extracting the experimental cutting force values required for the estimation of cutting constant. The subsequent subsections elaborate on these approaches with appropriate modifications for the consistency and clarity.

3.3.1 Approach 1: Average Cutting Constants

Wan et al. [2008a] proposed a systematic procedure to determine average cutting constants directly from the measured force without any pre-processing. This approach uses experimentally measured forces at a given cutter rotation angle, $F_s^m(\phi_i)$ $(s = X,Y)$ to determine cutting constants using Eq. 3.8. It is important to note that the measurement of experimental cutting forces at the element level $F_s^m(i,j,k)$ $(s = X,Y)$ is not feasible at the present. The experiments will provide the total cutting forces $F_s^m(\phi_i)$ $(s = X,Y)$, acting in X- and Y- direction at a given instance viz. cutter rotation angle (ϕ_i). The measured cutting forces $F_s^m(\phi_i)$ $(s = X,Y)$ are substituted in Eq. 3.8 to determine cutting constant $K_q(\phi_i)$ $(q = T,R)$ at the cutter rotation angle (ϕ_i).

$$\begin{bmatrix} F_X^m(\phi_i) \\ F_Y^m(\phi_i) \end{bmatrix} = dz \begin{bmatrix} \sum_{j,k} cos\beta(i,j,k)\, t_c(i,j,k) & -\sum_{j,k} sin\beta(i,j,k)\, t_c(i,j,k) \\ \sum_{j,k} sin\beta(i,j,k)\, t_c(i,j,k) & \sum_{j,k} cos\beta(i,j,k)\, t_c(i,j,k) \end{bmatrix} \begin{bmatrix} K_T(\phi_i) \\ K_R(\phi_i) \end{bmatrix} \tag{3.8}$$

The process of determining cutting constants $K_q(\phi_i)$ $(q = T,R)$ is to be repeated for one complete revolution of the cutter. The relationship between $K_q(\phi_i)$ $(q = T,R)$ and average chip thickness at various angular rotations of the cutter $t_{avg}(\phi_i)$ is expressed using Eq. 3.9. The coefficients of relationship can be determined using a non-linear curve fitting technique. The average chip thickness $t_{avg}(\phi_i)$ at each cutter rotation angle (ϕ_i) is computed using Eq. 3.10. The approach proposes averaging of the chip thickness at discrete cutter rotation angle using $w(i,j,k)$ as a weighting factor given by Eq. 3.11. The relationship between $K_q(\phi_i)$ and $t_{avg}(\phi_i)$ is used to predict cutting forces subsequently by replacing $K_q(i,j,k)$ $(q = T,R)$ and $t_c(i,j,k)$ in Eq. 3.9 to obtain instantaneous cutting forces acting on each disk element. The relationship between instantaneous chip thickness and cutting constants used in the determination of cutting force is expressed using Eq. 3.12.

$$K_q(\phi_i) = a_q\, e^{-b_q\, t_{avg}(\phi_i)} + c_q \qquad (q = T,R) \tag{3.9}$$

$$t_{avg}(\phi_i) = \frac{\sum_{j,k} t_c(i,j,k)\ \ w(i,j,k)}{\sum_{j,k}\ w(i,j,k)} \tag{3.10}$$

$$w(i,j,k) = \frac{j\, dz\, tan\,(\theta_h)}{R_c} \tag{3.11}$$

$$K_q(i,j,k) = a_q\, e^{-b_q\, t_c(i,j,k)} + c_q \qquad (q = T,R) \tag{3.12}$$

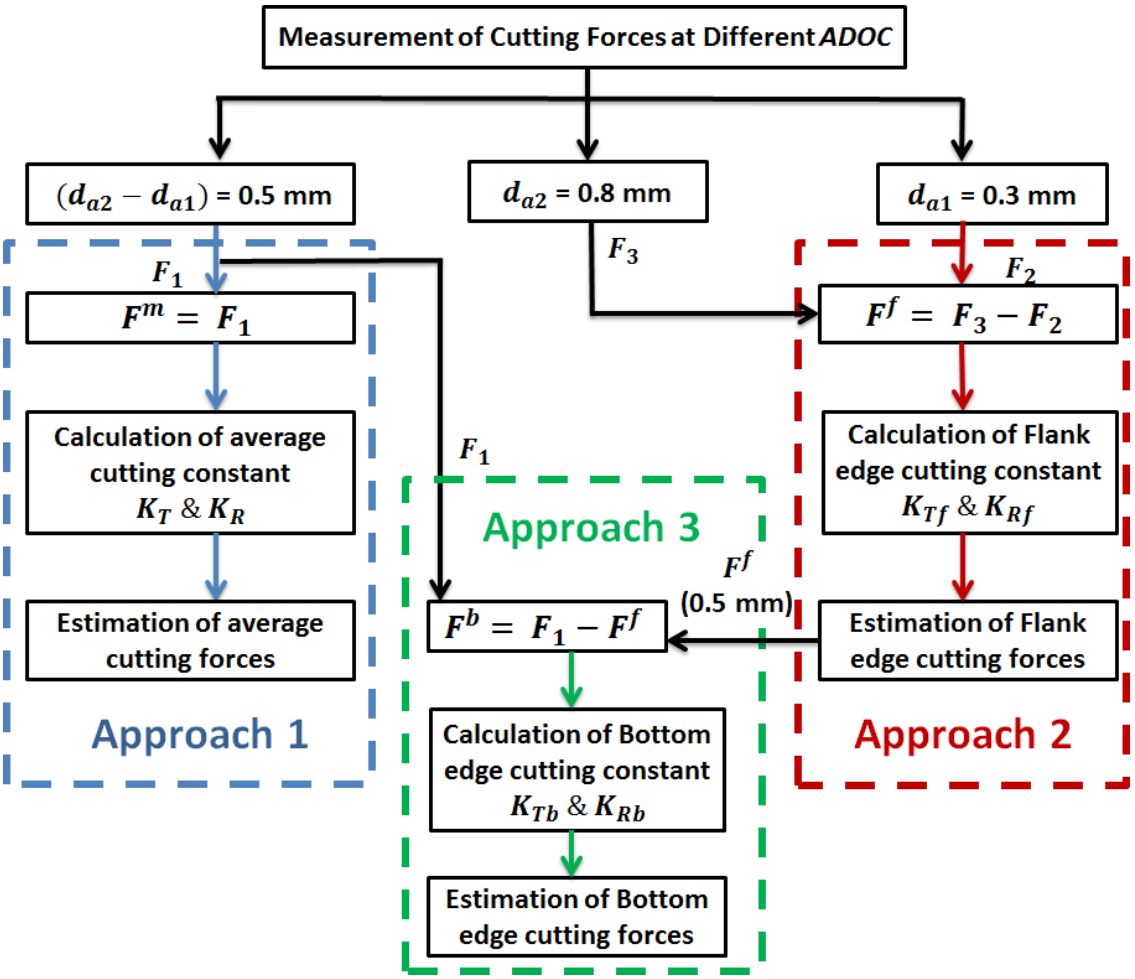

Figure 3.3 : Flowchart showing Comparison of Different Analytical Approaches

3.3.2 Approach 2: Instantaneous Flank Edge Constants

Ko et al. [2002] highlighted that the flank edge is a significant contributor to the total force, and the inclusion of data associated with the bottom edge while establishing cutting constant relationship lowers the prediction accuracy. The study proposed exclusion of the bottom edge data systematically from the measured cutting force signal while determining flank edge constants. Figure 3.3 shows a two-step procedure to exclude cutting force data related to the bottom edge from the measured signal. The first step proposes to conduct machining experiments and recording of cutting force data at two different $ADOC$ (d_{a1} & d_{a2}) with identical $RDOC$ and feed rate. The second step proposes synchronization and pre-processing of the cutting force data. The synchronization process requires adjustment of phases between both measured force signals. The synchronization follows pre-processing stage involving subtraction of forces measured at smaller $ADOC$ (d_{a1}) from the larger $ADOC$ (d_{a2}) to exclude the contribution of the bottom cutting edge from the experimental data. The cutting forces obtained after the subtraction are associated with a flank cutting edge $F_s^{mf}(\phi_i)$ $(s = X,Y)$ only and used for determining cutting coefficients $K_{qf}(\phi_i)$ $(q = T,R)$

using Eq. 3.13. The subsequent steps determining the relationship between cutting constant $K_{qf}(i,j,k)$ $(q = T,R)$ and instantaneous uncut chip thickness $t_c(i,j,k)$ are similar to the approach discussed in the Section 3.3.1. Equation 3.14 shows analytical expressions to determine flank forces $F_s^f(\phi_i)$ $(s = X,Y)$ at a cutter rotation angle (ϕ_i).

$$\begin{bmatrix} F_X^{mf}(\phi_i) \\ F_Y^{mf}(\phi_i) \end{bmatrix} = dz \begin{bmatrix} \sum_{j,k} cos\beta(i,j,k)\, t_c(i,j,k) & -\sum_{j,k} sin\beta(i,j,k)\, t_c(i,j,k) \\ \sum_{j,k} sin\beta(i,j,k)\, t_c(i,j,k) & \sum_{j,k} cos\beta(i,j,k)\, t_c(i,j,k) \end{bmatrix} \begin{bmatrix} K_{Tf}(\phi_i) \\ K_{Rf}(\phi_i) \end{bmatrix} \tag{3.13}$$

$$\begin{bmatrix} F_X^{f}(\phi_i) \\ F_Y^{f}(\phi_i) \end{bmatrix} = \sum_{j,k} dz \begin{bmatrix} cos\beta(i,j,k)\, t_c(i,j,k) & -sin\beta(i,j,k)\, t_c(i,j,k) \\ sin\beta(i,j,k)\, t_c(i,j,k) & cos\beta(i,j,k)\, t_c(i,j,k) \end{bmatrix} \begin{bmatrix} K_{Tf}(\phi_{i,j,k}) \\ K_{Rf}(\phi_{i,j,k}) \end{bmatrix} \tag{3.14}$$

3.3.3 Approach 3: Independent Flank and Bottom Edge Constants

Dang et al. [2010] demonstrated the significance of bottom cutting edge on cutting forces for certain cutting conditions, e.g., small *ADOC*. The study showed that the contribution of the bottom cutting edge is small on total cutting forces but it cannot be neglected in the model. The forces contributed by the flank edge are determined similarly to the previous approach. However, the forces contributed by the bottom edge are included in the model independently. Figure 3.3 depicts the process for extracting the bottom edge forces to estimate associated cutting constants. The study assumes a linear relationship between uncut chip thickness associated with the bottom disk element and cutting constant. The cutting force data corresponding to the bottom edge can be determined by subtracting flank force $F_s^f(\phi_i)$ $(s = X,Y)$ determined using Eq. 3.14 from experimentally measured cutting forces $F_s^m(\phi_i)$ $(s = X,Y)$ estimated for *ADOC* $(d_{a2} - d_{a1})$ after synchronization of the phase for each cutter rotation angle (ϕ_i). The expressions determining cutting force associated with the bottom edge are expressed using Eq. 3.15. The bottom edge cutting constant $K_{qb}(\phi_i)$ $(q = T,R)$ at (ϕ_i) can be determined by substituting the forces in Eq. 3.16 for the bottom-most disk element $(j = 1)$. The constant corresponding to the bottom edge is determined as an arithmetic mean of values at each cutter rotation angle for one revolution of the cutter expressed using Eq. 3.17. The cutting force components acting on the bottom edge can be computed using Eq. 3.18. The total cutting force at a given cutter rotation angle $F_s^T(\phi_i)$ $(s = X,Y)$ are determined by adding bottom edge force (F_s^b) and flank force (F_s^f) acting on each disk element and it is expressed using Eq. 3.19.

$$\begin{bmatrix} F_X^{mb}(\phi_i) \\ F_Y^{mb}(\phi_i) \end{bmatrix} = \begin{bmatrix} F_X^{m}(\phi_i) \\ F_Y^{m}(\phi_i) \end{bmatrix} - \begin{bmatrix} F_X^{f}(\phi_i) \\ F_Y^{f}(\phi_i) \end{bmatrix} \tag{3.15}$$

$$\begin{bmatrix} F_X^{mb}(\phi_i) \\ F_Y^{mb}(\phi_i) \end{bmatrix} = dz \begin{bmatrix} \sum_{j,k} cos\beta(i,j,k)\, t_c(i,j,k) & -\sum_{j,k} sin\beta(i,j,k)\, t_c(i,j,k) \\ \sum_{j,k} sin\beta(i,j,k)\, t_c(i,j,k) & \sum_{j,k} cos\beta(i,j,k)\, t_c(i,j,k) \end{bmatrix} \begin{bmatrix} K_{Tb}(\phi_i) \\ K_{Rb}(\phi_i) \end{bmatrix} \tag{3.16}$$

$$K_{qb} = avg\,(K_{qbi}) \qquad (q = T,R) \tag{3.17}$$

$$\begin{bmatrix} F_X^{b}(\phi_i) \\ F_Y^{b}(\phi_i) \end{bmatrix} = \sum_{j,k} dz \begin{bmatrix} cos\beta(i,j,k)\, t_c(i,j,k) & -sin\beta(i,j,k)\, t_c(i,j,k) \\ sin\beta(i,j,k)\, t_c(i,j,k) & cos\beta(i,j,k)\, t_c(i,j,k) \end{bmatrix} \begin{bmatrix} K_{Tb}(\phi_{i,j,k}) \\ K_{Rb}(\phi_{i,j,k}) \end{bmatrix} \tag{3.18}$$

$$F_s^T(\phi_i) = F_s^f(\phi_i) + F_s^b(\phi_i) \qquad (s = X, Y) \tag{3.19}$$

The consistency of the relationship between chip thickness and cutting constants obtained using the aforementioned analytical approach is dependent on the accuracy of the best fit curve obtained using the data points. These data points are prone to have numerous uncertainties and noisy values as they are extracted from the machining experiments. In order to improve the fitness of these relationships several attempts were reported in the literature such as excluding the "*size effect*" [Ko et al., 2002], removal of "*jump points*" at lower chip thickness region [Wan et al., 2008a], extraction of different relationships for "*bottom and flank edge*" [Dang et al., 2010], etc. However, limitations associated with the curve fitting techniques might result in the poorly fitted relationship that deteriorates the overall prediction accuracy of the cutting force model. In the subsequent subsection, a novel machine learning-based approach is discussed to replace the analytical relationship by overcoming these limitations.

3.4 MACHINE LEARNING-BASED APPROACH FOR CUTTING CONSTANT

This section presents a data-driven approach employing ANNs in establishing the non-linear relationship between cutting constants and instantaneous uncut chip thickness. The mathematical formulations to compute cutting constants $K_q(\phi_i)$ $(q = T, R)$ and average chip thickness $t_{avg}(\phi_i)$ values at different cutter rotation angle (ϕ_i) is identical to the approach discussed in Section 3.3.1. The determination of a non-linear relationship using curve fitting is replaced with the supervised ANN to learn the behaviour similar to the human brain. The supervised ANN model uses known combinations of $t_{avg}(\phi_i)$ (as an input) and $K_q(\phi_i)$ $(q = T, R)$ (as outputs) to learn the relationship using an architecture depicted in Figure 3.4. The ANN is a computational model of a human brain that acquires knowledge of performing a certain task by learning through examples instead of being programmed. The ANN consists of processing constituents termed as neurons, which develops a regulated network by identifying casual relationships among input and output. The neurons are organized in well-structured layers such as an input layer, one or a few hidden layers and an output layer. The present work necessitates an input layer consisting of a single neuron representing $t_{avg}(\phi_i)$ and the output layer comprising of two neurons representing $K_q(\phi_i)$ $(q = T, R)$.

The study employs a multi-layer feed-forward ANN, which transfers the information through a network of interconnected neurons from the input layer to the output layer via hidden layers. The output value of a neuron $(x_{p,q})$ for layer (p) is determined by weighted sum of neurons corresponding to the previous layer $(p-1)$ as Eq. 3.20. The term σ represents the activation function, which transforms linear input to the non-linear output value. Several activation functions are recommended in the literature, e.g., sigmoid, hyperbolic tangent, Rectified Linear Unit (RELU), etc. The sigmoid function normalizes output between $[0, 1]$ and causes the vanishing of the gradient at higher and lower input values. It results in increased time for the network to obtain accurate predictions. The convergence rate of a network is better when the RELU activation function is used. The gradient of the function converges to zero when inputs are near zero or negative and the network cannot learn by performing backpropagation. The present study employs hyperbolic tangent (*tanh*) function as an activation function to normalize output value between $[1, 1]$. The hyperbolic tangent activation function is advantageous as it provides the convenience of mapping model inputs to strongly negative and positive values. The activation function affects the overall performance of ANN by introducing non-linear properties. If the activation function is not applied, the model would behave linear and will not learn the complex behaviour of the end milling system. The term *bias* is added to improve the flexibility of ANN by varying the intercept of the regression line. The number of hidden layers and neurons in each layer is determined iteratively based on

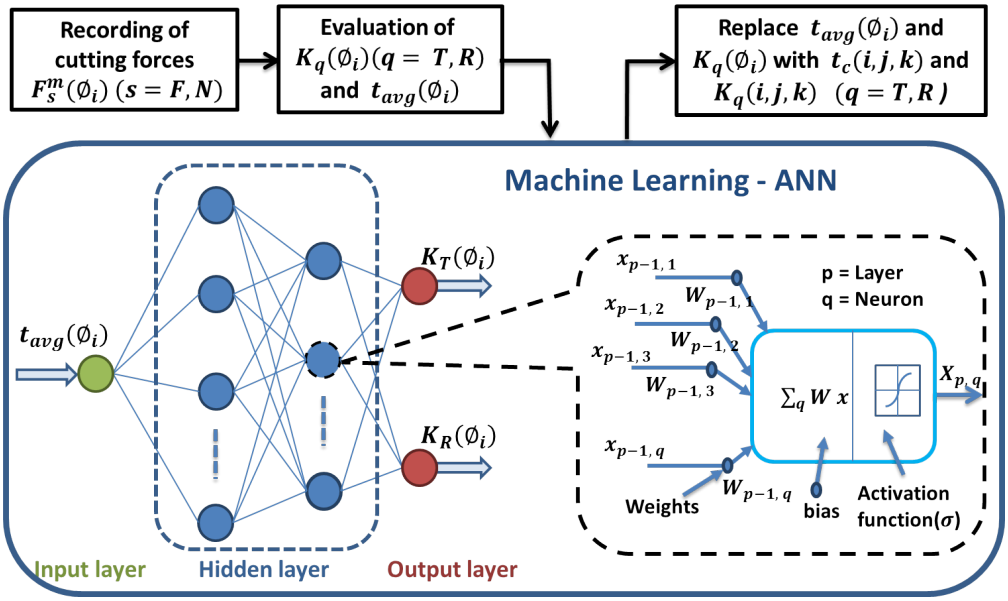

Figure 3.4 : Flowchart for Calibration of Cutting Constant using Machine Learning

the performance of the ANN. The satisfactory performance was observed with a network having two hidden layers having 20 and 10 neurons, respectively.

$$x_{p,q} = \sigma \sum_{q} W_{p-1,q}\, x_{p-1,q} + bias \tag{3.20}$$

$$E = \sum_{i=1}^{k} (t_i - y_i)^2 \qquad k = Number\ of\ datasets \tag{3.21}$$

$$W_{p,q}^{n+1} = W_{p,q}^{n} + \alpha \frac{\partial E}{\partial W_{p,q}} \tag{3.22}$$

The training of ANN is accomplished using the Levenberg-Backpropagation algorithm in combination with Bayesian regularization [MacKay, 1992]. This algorithm is ideal for regression problems as in the present study owing to its efficiency and ability to optimize weight distribution for avoiding overfitting of the network [Kayri, 2016]. The training was initiated using random weights $(W_{p,q})$ associated with each neuron. The input data is fed to the network to predict the output (y) which is compared subsequently with the actual value of a target (t). The square of the difference between predicted (y) and target output (t) value termed as an error (E) is backpropagated through the network to alter the weights of the neurons using Eq. 3.21 and 3.22. Here, α is the learning rate that regulates the step size of the gradient for the subsequent iteration. The backpropagation process is reiterated until the maximum number of iterations (n) was reached.

The ANN model is validated using testing datasets after completing the training without providing the output vector. If the estimation with output dataset is satisfactory, the developed ANN model can be applied to prediction of instantaneous cutting constants $K_q(i,j,k)$ $(q = T, R)$ corresponding to input values of instantaneous uncut chip thickness $t_c(i,j,k)$. The values of $t_c(i,j,k)$ computed from analytical model can be substituted in ANN to predict cutting forces $F_s^m(\phi_i)$ $(s = F, N)$. Figure 3.4 summarizes the overall procedure of estimating cutting constants and forces using the proposed approach.

3.5 DETERMINATION OF CUTTING CONSTANTS

The analytical and machine learning-based approaches outlined in the previous section are implemented in the form of computational programs using MATLAB 2019b [2019] to establish cutting constant relationships. The present section summarizes the procedure for determining the coefficients of the relationship of cutting constants expressed using Eqs. 3.9, 3.12, and 3.17. Subsequently, an ANN driven machine learning approach is developed to establish the non-linear relationship between instantaneous uncut chip thickness and cutting constants. In order to accomplish these objectives, machining experiments are conducted on a 3-axis Vertical Milling Machine using the solid carbide end mill and Aluminium 6061-T6 workpiece material with other cutting conditions summarized in Table 3.2. The end mill with a small overhang is clamped in a rigid tool holder with the negligible cutter runout to minimize the effect of tool deflections on cutting forces. The experiments employed a combination of cutting widths and lower spindle speeds to ensure stable conditions and reduction of machining chatter. The cutting forces are recorded as a function of cutter rotation angle using Kistler 9257B table Dynamometer and data acquisition system with software. Figure 3.5 shows the experimental set up used for end milling experiments during the present thesis work.

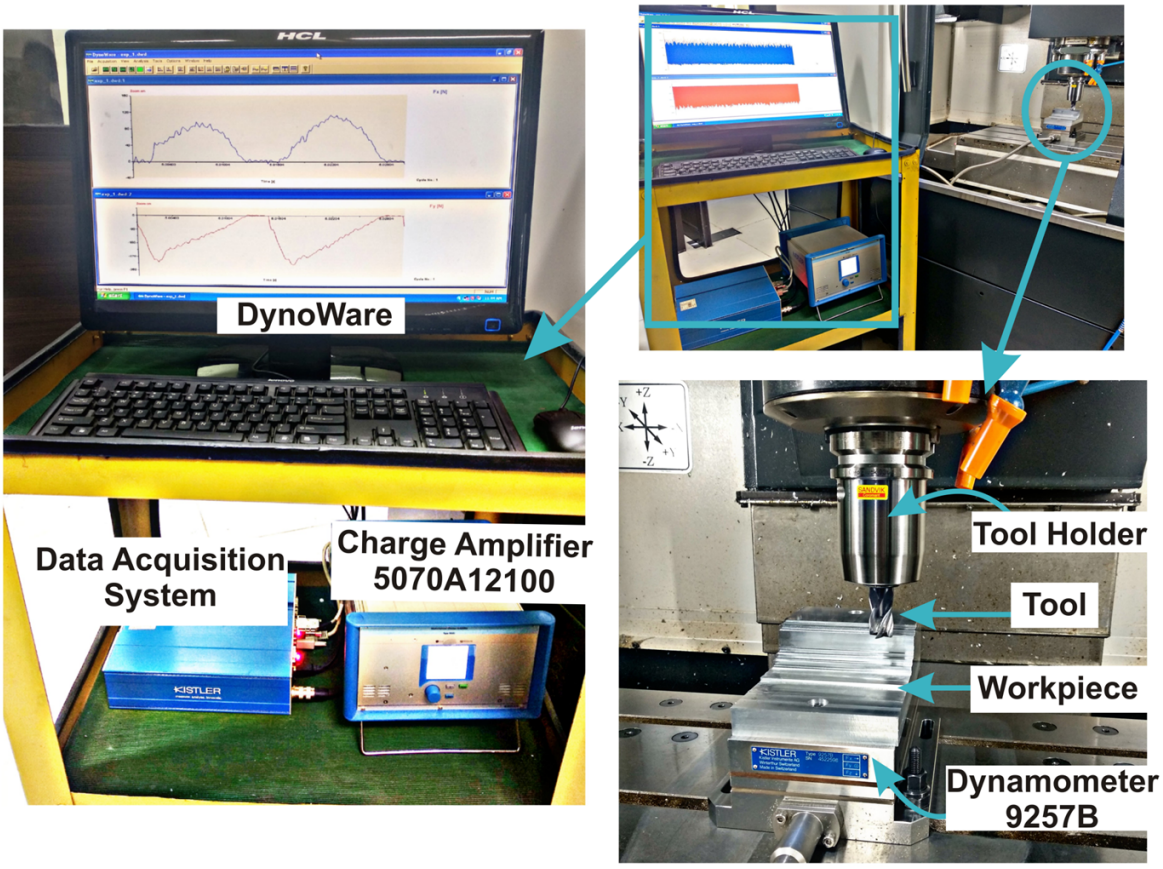

Figure 3.5 : Experimental Setup

3.5.1 Analytical Approaches

The cutting conditions corresponding to the first set (Table 3.2) are used for the determination of average cutting constants (approach 1). The cutting forces are recorded as a function of cutter rotation angle (ϕ_i) for one revolution of the cutter. The values of cutting constants $K_q(\phi_i)$ $(q = T, R)$ and $t_{avg}(\phi_i)$ at different instants of cutter rotation are determined using Eqs. 3.8 and 3.10 respectively. Figures 3.6a and 3.6b show values of $K_q(\phi_i)$ $(q = T, R)$ and $t_{avg}(\phi_i)$ at

different cutter rotation angles calculated using Eqs. 3.8 and 3.10. It can be seen that the values of $K_q(\phi_i)$ $(q = T, R)$ are significantly larger when uncut chip thickness is small due to *"size effect"*. The mathematical relationship between $K_q(\phi_i)$ $(q = T, R)$ and $t_{avg}(\phi_i)$ is determined using a non-linear curve fitting technique. Figures 3.6a and 3.6b show the non-linear relationship along with value of coefficients used for the prediction of cutting forces using approach 1.

Table 3.2 : Machining Conditions for Determination of Constants

Test No.	*RDOC* (mm)	*ADOC* (mm)	Feed (mm/min)
1	6	0.5 $(d_{a2} - d_{a1})$	400
2	6	0.3 (d_{a1})	400
3	6	0.8 (d_{a2})	400
Workpiece	:	Aluminium 6061-T6	
Tool	:	Solid Carbide (Kennametal - 4CH1600DK022A)	
Spindle Speed	:	2000 RPM	
Cutter Diameter	:	16 mm	
No. of Flutes	:	4	
Helix Angle	:	30°	

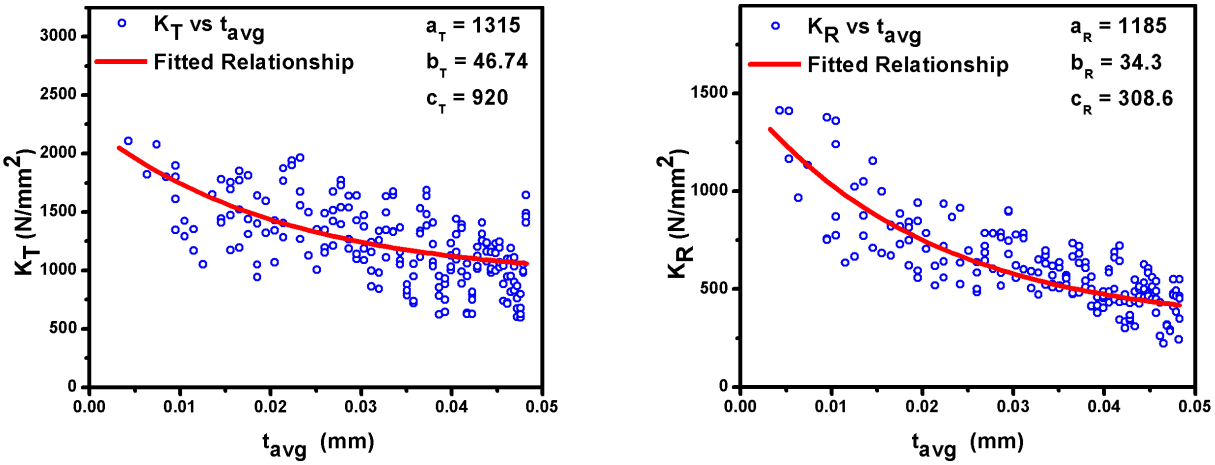

(a) K_T *vs* t_{avg} **(b)** K_R *vs* t_{avg}

Figure 3.6 : Average Cutting Constants (Approach 1)

The second approach requires conducting machining experiments and recording of the measured cutting force data at two different values of *ADOC* (d_{a1} and d_{a2}) with other cutting conditions maintained at the same level. The machining conditions corresponding to set 2 and 3 (Table 3.2) are used to derive cutting constants using approach 2. The recorded force data is synchronized for the adjustment of phases before pre-processing. The cutting forces measured at smaller *ADOC* ($d_{a1} = 0.3\ mm$) are subtracted from the ones at larger *ADOC* ($d_{a2} = 0.8\ mm$) subsequently. The subtraction process determines measured cutting forces associated with the flank edge $F_s^{mf}(\phi_i)$ which is used further to determine flank edge coefficients. The subsequent process for deriving values of $K_{qf}(\phi_i)$ $(q = T, R)$ and $t_c(\phi_i)$ is similar to the approach 1. Figures 3.7a and 3.7b show cutting constant values determined using Eq. 3.13 along with fitted relationships and values of coefficients.

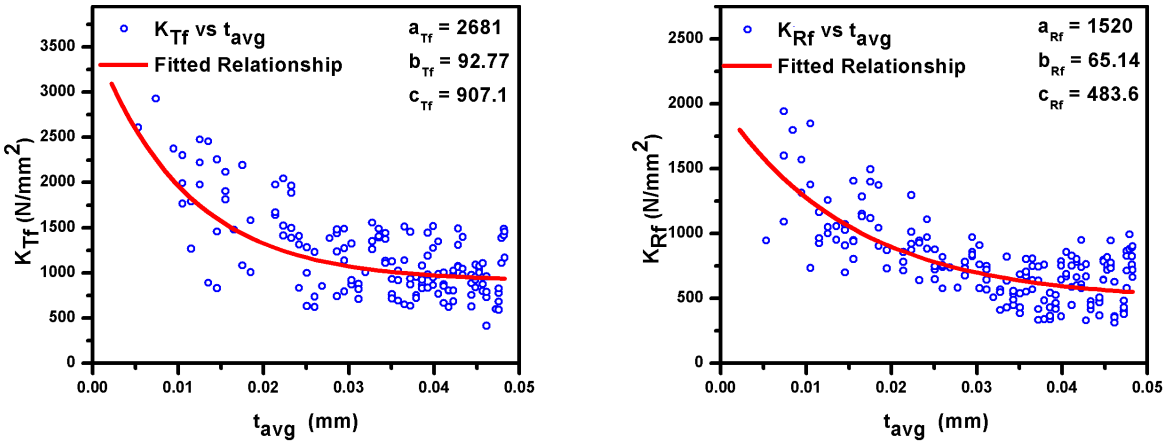

(a) K_{Tf} *vs* t_{avg} (b) K_{Rf} *vs* t_{avg}

Figure 3.7 : Flank Edge Cutting Constants (Approach 2)

The third approach requires the computation of independent flank and bottom edge cutting constants. The method adopts a constant relationship derived using approach 2 to estimate forces contributed by the flank edge. The flank forces calculated for conditions corresponding to set 1 (Table 3.2) are subtracted from experimentally measured forces to determine bottom edge forces. The bottom edge forces are substituted in Eq. 3.16 with $j = 1$ to calculate bottom edge coefficients $K_{qb}(\phi_i)$ $(q = T, R)$. Figures 3.8a and 3.8b show bottom edge cutting coefficients along with the fitted relationship computed as the arithmetic mean of cutting constant values corresponding to each data point. The broader spread of the data-points in Figure 3.8 is due to the bottom edge rubbing with the component. The total cutting force at the given cutter rotation angle is determined by the summation of flank and bottom edge cutting forces.

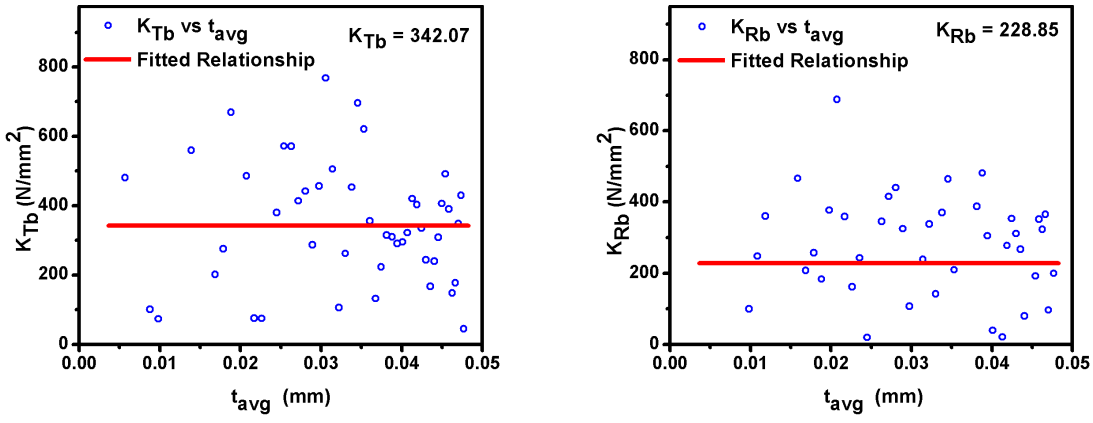

(a) K_{Tb} *vs* t_{avg} (b) K_{Rb} *vs* t_{avg}

Figure 3.8 : Bottom Edge Cutting Constants (Approach 3)

3.5.2 Machine Learning Approach

The machine learning toolbox of MATLAB 2019b [2019] has been used to develop the ANN model outlined in Section 3.4 for determining cutting constant relationships. The test 3 is used to train the ANN model as it requires a large number of datasets for effective extraction of the

relationship between input and output parameters. The cutting forces were recorded at a higher frequency of 3600 readings per revolution for cutting conditions corresponding to Test 3 (Table 3.2). The forces associated with one flute of the cutter (900 readings) are used to determine $K_q(\phi_i)$ $(q = T, R)$ and $t_{avg}(\phi_i)$ using Eqs. 3.8 and 3.10 respectively. The flute is partially engaged in the cut during test 3 which yielded about 786 discrete combinations of $K_q(\phi_i)$ $(q = T, R)$ and $t_{avg}(\phi_i)$ that are chosen as the training datasets. The dataset obtained was normalized between [0, 1] using the Max-Min method and rearranged randomly before dividing into training (70%) and testing (30%) datasets. The datasets were presented to the ANN model using topology summarized in Section 3.4. Figures 3.9a and 3.9b shows the performance and regression plots obtained for the ANN model developed in the present study.

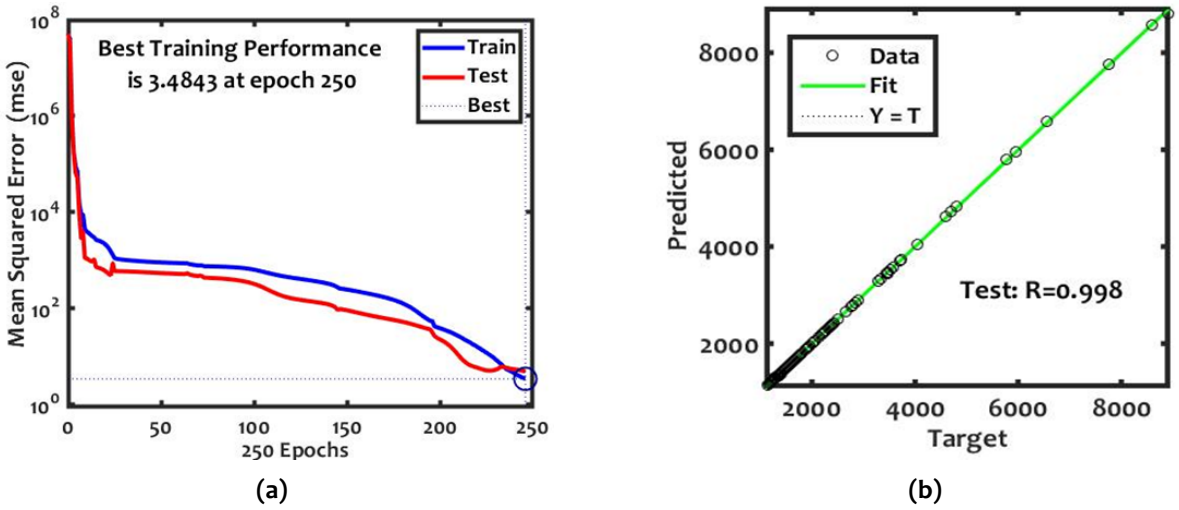

Figure 3.9 : ANN Model - (a) Performance Plot and (b) Regression Plot

3.6 COMPUTATIONAL AND EXPERIMENTAL RESULTS

The mechanistic force model discussed in Section 3.2 has been implemented in the form of computational program using MATLAB 2019b [2019] to predict cutting forces during end milling operation over a range of cutting widths i.e. *ADOC* and *RDOC*. The relationships between mechanistic cutting constants and uncut chip thickness derived using analytical and machine learning approaches outlined in Sections 3.3-3.5 are used to estimate cutting constant relationship. Thereafter, a series of end milling experiments are conducted to examine the effectiveness of these approaches in predicting cutting forces under various machining conditions. The attributes related to the experimental setup, cutting tool and workpiece are kept identical as outlined in Section 3.5. Table 3.3 summarizes the values of *ADOC* and *RDOC* used during tests with other cutting conditions similar to Table 3.2.

Table 3.3 : Machining Conditions for Experimental Verification

Test No.	*RDOC* (mm)	*ADOC* (mm)	Feed (mm/min)	Remarks
1	2	2	400	Constant *ADOC*
2	6	2	400	(lower value)
3	1.5	4	400	Constant *RDOC*
4	1.5	10	400	(lower value)
5	4	10	400	Higher *ADOC* and
6	6	6	400	*RDOC* (Roughing)

3.6.1 Performance Assessment of Analytical Approaches

Figures 3.10 and 3.11 present a comparison of cutting forces predicted using three different approaches with experimentally measured values for cutting conditions corresponding to Test 1 and 2 (Table 3.3). The objective of these tests is to examine the prediction ability of these approaches with the change of *RDOC* at lower *ADOC* values.

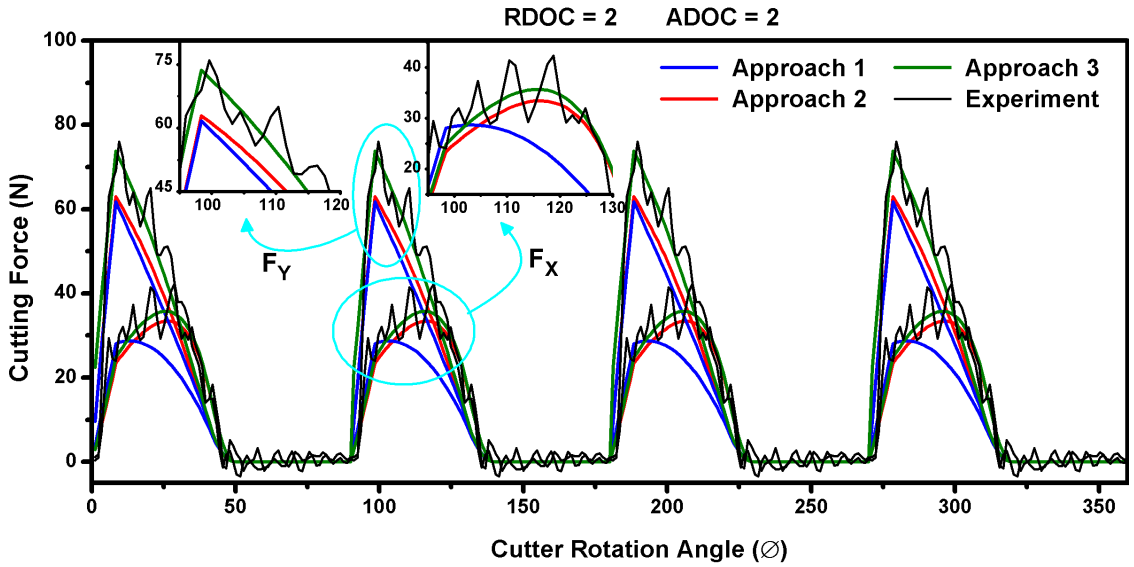

Figure 3.10 : Comparison of Measured and Predicted Forces (Test 1)

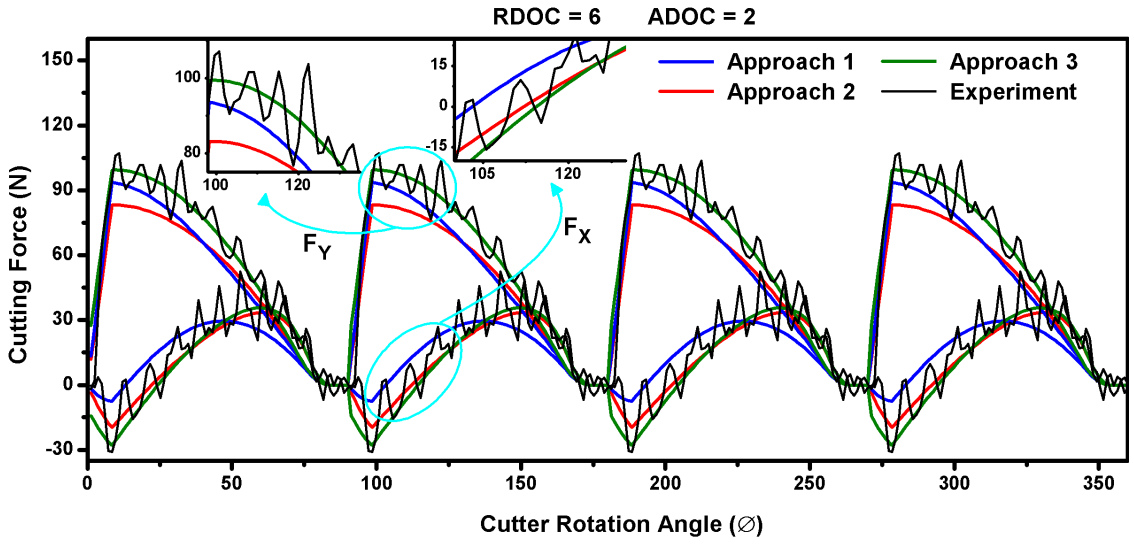

Figure 3.11 : Comparison of Measured and Predicted Forces (Test 2)

It can be seen that approach 3 considering independent flank and bottom edge cutting constants predict cutting forces accurately for both test cases. The prediction results of approaches 1 and 2 are comparable for Test 1. But, the prediction ability of the second approach incorporating flank edge constants is substantially lower compared to approach 1 considering average cutting constants for Test 2. The same can be attributed to larger *RDOC* and thereby substantial contribution from the bottom edge to the total cutting force. The approach 2 does not include bottom edge forces in the cutting force model, whereas approach 1 uses the raw data with the bottom edge contribution in predicting cutting constants. Based on the combined outcomes of

experiments and computational studies, it can be inferred that the contribution of the bottom edge is significant when a combination of larger *RDOC* and smaller *ADOC* is used during the flat-end milling operation. As approach 1 and 2 does not incorporate bottom edge effects independently into the model, it yields inferior prediction accuracy.

Figures 3.12 and 3.13 present a comparison of cutting forces predicted using three different approaches along with experimentally measured values for conditions corresponding to Test 3 and 4 (Table 3.3). The objective of these tests is to examine the prediction accuracy of these three approaches with the change of *ADOC* at lower *RDOC* values.

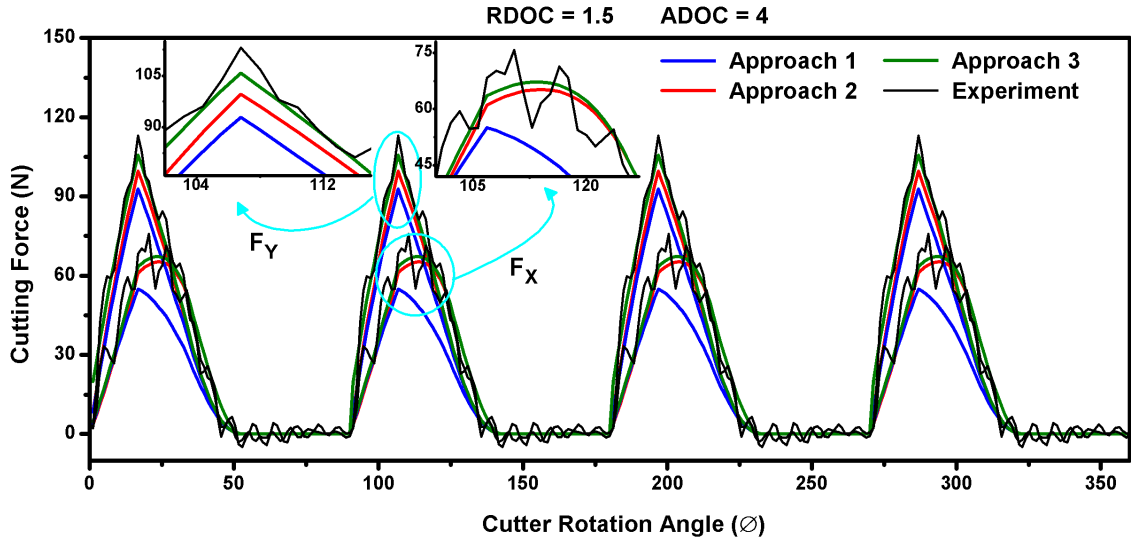

Figure 3.12 : Comparison of Measured and Predicted Forces (Test 3)

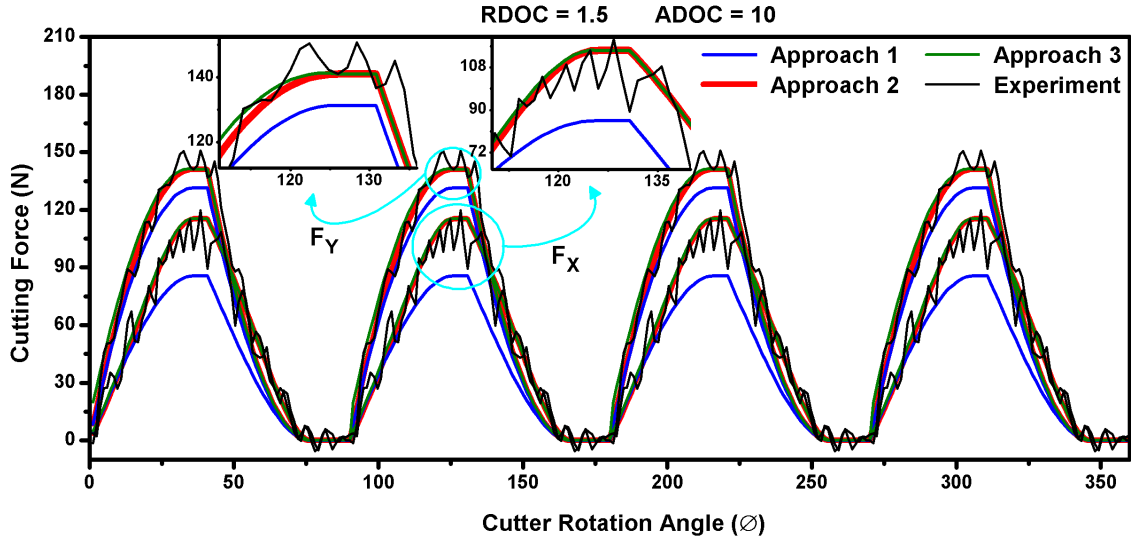

Figure 3.13 : Comparison of Measured and Predicted Forces (Test 4)

It can be seen that the forces predicted using approach 3 are in good agreement with measured values in comparison to the other two methods. The prediction accuracy of approach 2 is considerably better in this case in comparison to the cases involving higher *RDOC*. The smaller value of *RDOC* reduces the length of the bottom edge engaged in the cut lowering its contribution to the total forces during these tests. The same can be substantiated further using results shown in

Figure 3.13 which corresponds to Test 4 where *ADOC* is considerably large in comparison to Test 3. The contribution of flank edge forces is much higher in this case due to larger *ADOC* yielding almost identical predictions using approach 2 and 3. The slight deviations of F_X and F_Y among both methods are attributed to the engagement of the bottom edge at a particular instant. The prediction accuracy of approach 1 is the lowest for both these tests due to the use of combined flank and bottom edge force data while determining the single cutting constant relationship. The difference between instantaneous uncut chip thickness from bottom to top axial disk element is substantial for larger values of *ADOC*. It is not realistic to incorporate such variation into a single average constant which yields reduced prediction accuracy for approach 1.

Figures 3.14 and 3.15 show a comparison of cutting forces predicted using these three approaches with experimentally measured results for conditions corresponding to Test 5 and 6 (Table 3.3). The primary objective of these tests is to examine the prediction accuracy of approaches under roughing conditions, e.g., higher values of *ADOC* and *RDOC*.

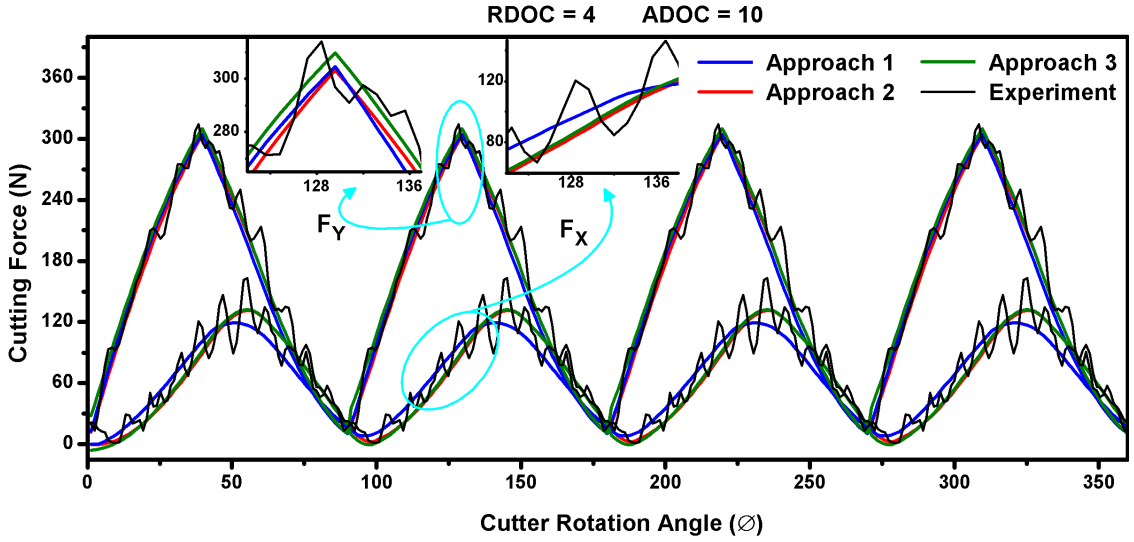

Figure 3.14 : Comparison of Measured and Predicted Forces (Test 5)

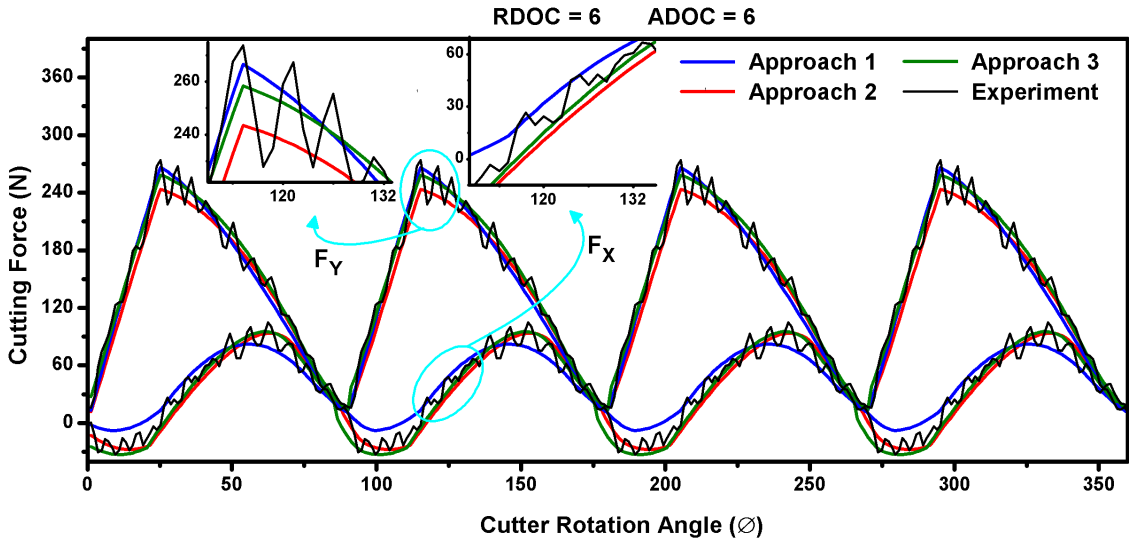

Figure 3.15 : Comparison of Measured and Predicted Forces (Test 6)

It can be seen that the contribution of the bottom edge is insignificant as the flank edge is a major contributor to the total cutting force. It results in identical cutting force predictions using approach 2 and 3 for roughing conditions. An important point to note is the variation of tangential force (F_X) predicted using approach 1 in both cases. It can be seen that the application of average cutting constants and raw force data in the determination of cutting constants have a significant influence on the prediction accuracy. The tangential force is not predicted accurately for both tests, while the other two approaches predict the same very well.

Based on the combined results for each test and various approaches presented above, it can be concluded that the bottom edge does not have a marked effect on the tangential force (F_X) as predictions are identical for each combination. Meanwhile, the influence of the bottom cutting edge on normal cutting force (F_Y) is significant and it must be incorporated independently in the model for the improved prediction accuracy. It justifies the fundamental contribution of this chapter to compare the prediction accuracy of three approaches, as the cutting force in normal direction contributes considerably towards the generation of distorted machined surface. Based on computational studies and experimental results conducted over a variety of cutting conditions, it can be concluded that analytical approach 3 predicts cutting forces very well over a wide range of cutting widths. The improved prediction accuracy of the model can be attributed to the independent inclusion of the bottom edge using separate cutting constants. Meanwhile, the prediction accuracy of the other two approaches is dependent on cutting widths, i.e., the poor prediction accuracy of approach 2 at higher *RDOC* and lower *ADOC* values. The development of generic model to estimate and control geometric tolerances during milling of thin-walled components in the subsequent chapters require accurate estimation of cutting forces over a range of cutting widths. Therefore, the reliable accuracy of approach 3 over a range of cutting widths enables it as a suitable approach.

3.6.2 Experimental Verification of Machine Learning Approach

The effectiveness of machine learning-based approach as an alternative to the analytical relationship between cutting constants and instantaneous uncut chip thickness is also examined by conducting end milling experiments. The cutting forces are estimated computationally using the approach outlined in section 3.5.2 and compared with the analytical approach applying independent constants for flank and bottom cutting edges (Approach 3) as well as experimental results.

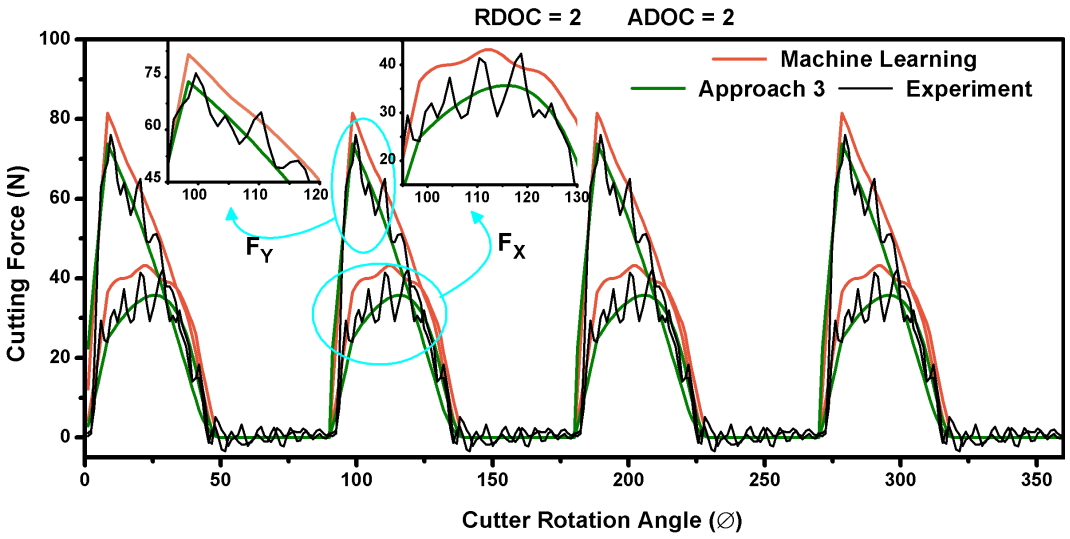

Figure 3.16 : Comparison of Predicted Forces from Analytical and Machine Learning Model (Test 1)

Figure 3.16-3.18 depicts the comparison of cutting forces predicted computationally using both approaches and experimentally measured values for conditions corresponding to Test 1,3 and 6 (Table 3.3). It can be observed from Figure 3.16-3.18, that the machine learning approach predicts the profile and magnitude of cutting forces accurately for all cases. Based on the outcomes of the present study, it can be inferred that the machine learning-based model is able to realize the relationship between uncut chip thickness and cutting constant effectively, thereby it can be used as an alternative to the analytical models employing non-linear curve fitting techniques. However, it is observed that the normal component (F_Y) of the cutting force is predicted consistently higher which needs further investigation and analysis. It can be explored as subsequent study of the present work by employing new generation machine learning models with better abilities.

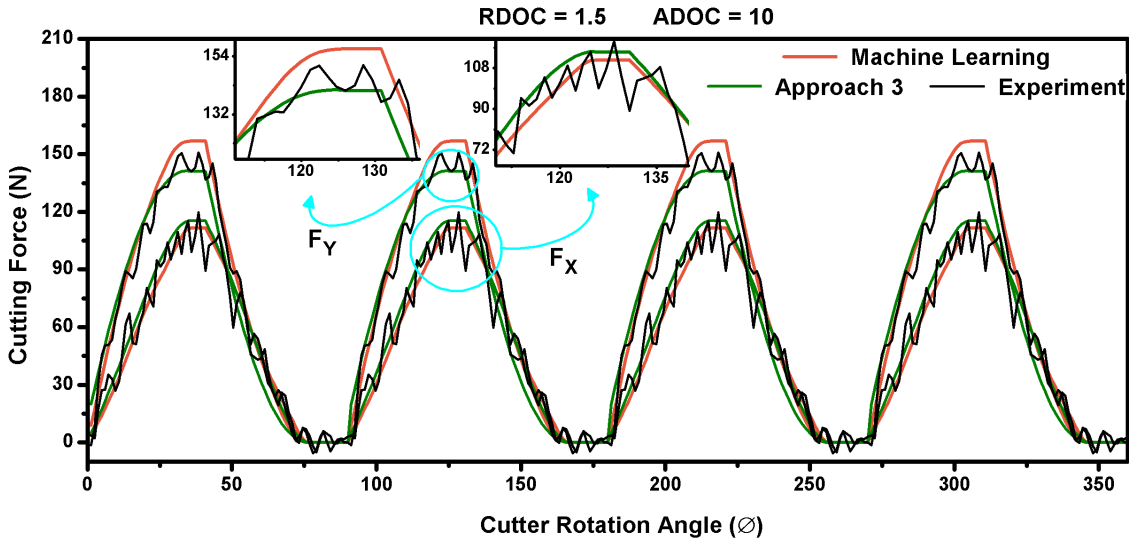

Figure 3.17 : Comparison of Predicted Forces from Analytical and Machine Learning Model (Test 3)

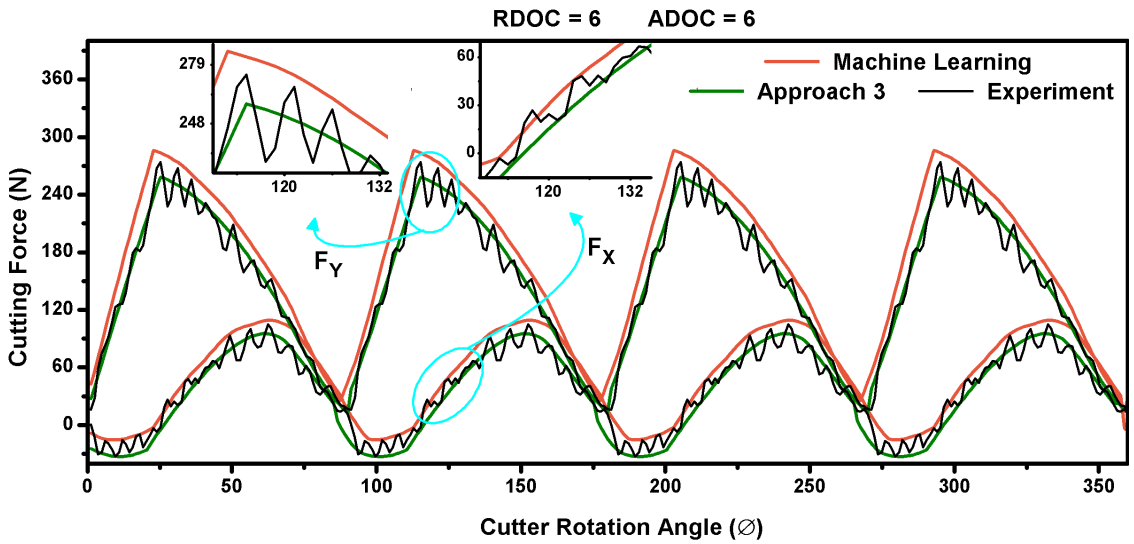

Figure 3.18 : Comparison of Predicted Forces from Analytical and Machine Learning Model (Test 6)

3.7 SUMMARY

This chapter presented different computational approaches for establishing cutting constant relationships during the end milling operation. Firstly, three different analytical approaches adopted from the literature are compared to highlight the importance of incorporating bottom and flank cutting edges in cutting force models for end milling operation. The study focuses on identifying the most appropriate method for predicting cutting forces over a range of cutting widths i.e., *ADOC* and *RDOC*. The first approach determines cutting constants directly from the experimental force data. The second approach pre-processes the experimental data to exclude the contribution of bottom edge and determines cutting constant associated with flank edge only. The third approach derive independent cutting constants for flank and bottom edges. The cutting constant obtained through the three analytical approaches are applied to predict cutting forces computationally and compared with experimentally measured values. The comparative assessment realizes the importance of both, bottom and flank edges towards cutting forces in the end milling over a range of cutting widths. Thereafter, a hybrid approach is presented that combines the strengths of the physics-based mechanistic model and machine learning to mimics the relationship between cutting constants and instantaneous uncut chip thickness. The hybrid approach was implemented in the form of computational programs and a series of machining experiments were carried out to examine the effectiveness of this approach in predicting cutting forces.

…